Three-dimensional morphology of nanoporous gold

doi: 10.1063/1.2948902

Three-dimensional morphology of nanoporous gold

Takeshi Fujita,[1] Li-Hua Qian,[1] Koji Inoke,[2] Jonah Erlebacher,[3] and Ming-Wei Chen[1,a)]
[1]*WPI Advanced Institute for Materials Research, Tohoku University, Sendai 980-8577, Japan*
[2]*FEI Company Japan Ltd., Minato-ku, Tokyo 108-0075, Japan*
[3]*Department of Materials Science and Engineering, Johns Hopkins University, Maryland 21218, USA*

(Received 22 April 2008; accepted 27 May 2008; published online 23 June 2008)

We report transmission electron tomography of nanoporous gold fabricated by chemically dealloying $Au_{35}Ag_{65}$ films. A number of algorithms were employed to quantitatively characterize the complex three-dimensional nanoporous structure. It was found that gold ligaments and nanopore channels are topologically and morphologically equivalent, i.e., they are inverses of each other in three-dimensional space. Statistical analysis reveals that this bicontinuous nanostructured material is actually quasiperiodic and has, on average, a near zero surface curvature. These quantitative measurements will help in understanding the structural stability of nanoporous gold and in modeling its physical and chemical performances. © *2008 American Institute of Physics*.
[DOI: 10.1063/1.2948902]

Nanoporous metals (pore size 5–50 nm) produced by selective chemical etching possess some of the most intricate and random three-dimensional (3D) morphologies. One example is nanoporous gold formed by dealloying silver from silver/gold alloys.[1] Porous metals formed by spontaneously dealloying, at first glance, appear to be completely irregular in morphology for both the pores and metallic ligaments comprising the nanostructure. Some investigations of the structure of dealloyed porous metals have been made using plan-view transmission electron microscopy (TEM) and scanning electron microscopy (SEM),[2,3] which cannot probe the internal microstructure. Neutron scattering was attempted to investigate the internal structure of nanoporous metals. However, the results strongly rely on generating statistical models to fit the scattering data and thus lose local morphological information.[4] More recently, transmission electron tomography has been employed to reveal the 3D structure of nanoporous gold.[5,6] Preliminary results of the reconstructed 3D configurations have shown great advantage of this real-space technique to illuminate the internal structure of nanoporous metals. Because of their distinctive properties, such as high surface-to-volume ratios, excellent electric and thermal conductivities, and open nanoporosity extending in three dimensions, nanoporous gold have recently begun to be exploited for a wide range of applications in catalysis, sensing, actuation, and biotechnology.[7–10] Therefore, quantitative information on the 3D structure of nanoporous metals becomes essential for modeling and optimizing their performances. In this study we employed electron tomography along with a number of algorithms to quantitatively characterize the complex 3D nanoporous structure of nanoporous gold made from an optimal precursor alloy composition of $Au_{35}Ag_{65}$.

Nanoporous gold membranes used in this study were prepared by chemical dealloying. Samples of ~100 nm thick white gold leaf ($Au_{35}Ag_{65}$, 50/50 by weight, Sepp Leaf Products, New York) were dealloyed when floated upon 70 vol % HNO_3 at room temperature for 5 min, which dissolves the silver from the leaf leaving behind a nanoporous gold membrane. After dealloying, samples were thoroughly rinsed with distilled water for microstructural characterization. The morphology of the nanoporous gold membranes was investigated by using a computer controlled scanning transmission electron microscope (Tecnai F30, FEI Co.) equipped with a high-tilt specimen holder. A series of high-angle annular dark field TEM images were acquired from −70° to +70° with an image recorded at every 2°. Probe current, dwell time, and mean detector counts were approximately 1 nA, 14 μs/pixels, and 40000, respectively. The tilt series were recorded automatically with XPLORE3D software (FEI). The 3D reconstruction was achieved by using INSPECT3D software (FEI) after off-line alignment for fine tuning by using a cross-correlation algorithm.

Figure 1(a) shows an example of three orthogonal crosscuts through the 3D reconstruction after a median filtering. The bright regions indicate the gold ligaments with high *Z* contrast. Obvious microstructure difference between the plan view (*XY* plane) and the side views (both *XZ* and *YZ* planes) of the porous nanostructure cannot be found, indicating that the miss wedge effect is not evident in the 3D reconstruction. In this study, the optimal threshold value for binarization was determined by careful comparison between slices of the binarized and reconstructed densities. With this procedure, a single threshold is determined from a middle image in the 3D dataset and applied to all images [Fig. 1(b)]. In the 3D reconstruction with the optimal threshold, all floating 3D segments that cannot exist in the real sample were treated as the artifacts that were eliminated by using TRI software (Rac-

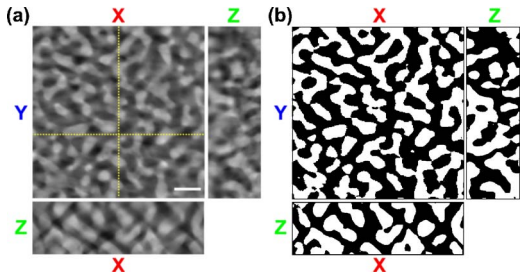

FIG. 1. (Color online) (a) Three orthogonal crosscuts through the 3D reconstruction. The scale bar is 50 nm. The two-dimensional image of the *X*-*Y* plane is the middle of 3D volume. The yellow cross lines represent the crosscut planes. (b) Binary images of (a) using the optimal cutoff threshold.

a)Author to whom correspondence should be addressed. Electronic mail: mwchen@imr.tohoku.ac.jp.

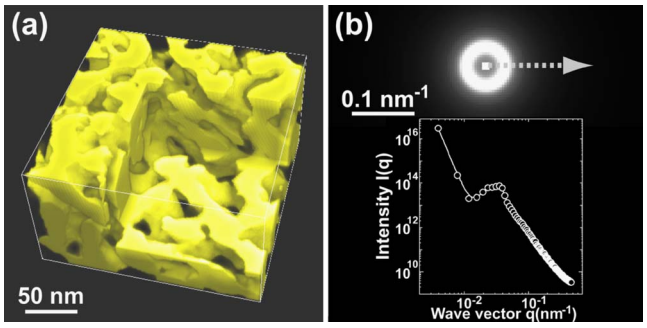

FIG. 2. (Color online) 3D tomographic reconstruction of nanoporous gold. (a) Magnified 3D image revealing the internal bicontinuous structure of nanoporous gold. (b) Fourier-transformed pattern showing the quasiperiodic feature of nanoporous gold. The inserted intensity profile was taken along the dash arrowhead in the Fourier-transform pattern.

toc, Japan). The resultant 3D volume is highly bifurcated at the interfaces, either it is dense (voxel near 100%) for gold ligaments or empty (voxel near 0%) for nanopore channels. Because the cutoff threshold strongly affects the quality of the 3D reconstruction, in particular, the quantitative measurements, the validity of the optimal threshold used in our study was assessed by the 3D volume ratio. The 3D volume ratio between gold ligaments and nanopore channels was calculated to be 11:12, in the reconstructed volume, which is very close to the 50:50 determined by electrochemical measurements and SEM characterization,[4,8] proving the validity of the cutoff. In addition to the volume assessment, the quantitative analyses reported in this letter, including the length scale and internal area, are all in agreement with the experimental data determined by other techniques (SEM, TEM, electrochemical measurements, and Monte Carlo simulations).[1,10,11] Accordingly, these assessments unambiguously prove the quality and reliability of our 3D reconstruction and the quantitative analyses.

Figure 2(a) shows a cutoff 3D image that exposes the internal structure of the nanoporous gold. The interconnections of the gold ligaments and nanopore channels in 3D confirm that nanoporous gold possesses a bicontinuous 3D structure with a random shape for both nanopores and gold ligaments. However, the Fourier-transformed pattern of the volumetric dataset, produced by a rotational averaging to eliminate background noise[11] [Fig. 2(b)], shows that the sample possesses a characteristic length scale $L \sim 30$ nm that is associated with a statistical period length of the structure and equals the sum of the average ligament diameter and average pore diameter. Thus, the average radius for both ligaments and nanopores was estimated to be ~7.5 nm. Additionally, the surface area of the gold ligaments in the nanoporous structure was calculated by using a Marching-cube algorithm.[12] The total specific surface area calculated by summing all the surface triangles was measured to be ~12 m^2/g, which is fairly consistent with the electrochemical measurements of the active internal surface area (~9–11 m^2/g).[13]

In order to quantitatively characterize the morphology of nanoporous gold in three dimensions, we used a number of algorithms to uncover the structural characteristics of the complex bicontinuous material. First, we measured the length and diameter distributions of gold ligaments and nanopore channels. This was accomplished by translating the nanostructure into a skeletal network using a 3D thinning

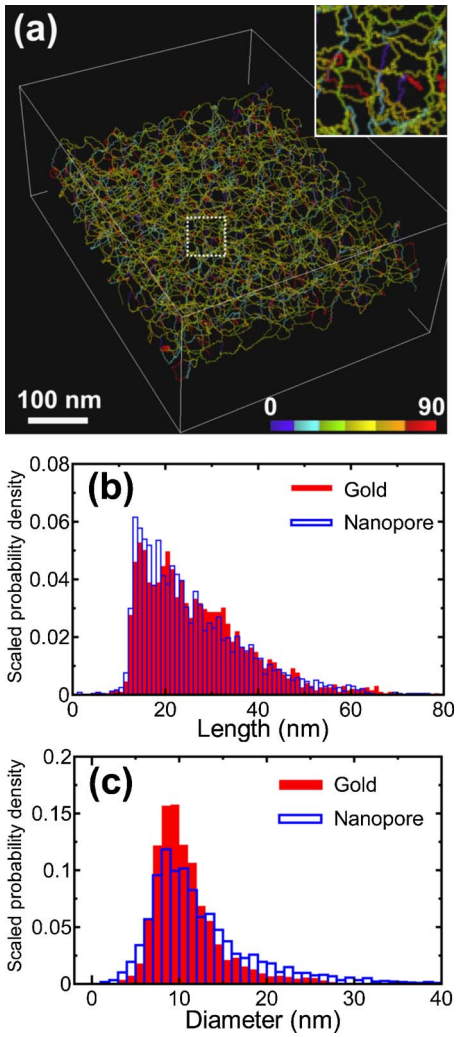

FIG. 3. (Color online) Quantitative length scale measurements. (a) Skeletal network of gold ligaments generated by using a 3D thinning algorithm. The insert shows a zoom-in image of the skeletal network with structural details. (b) Histograms of scaled probability density of interjunction path length of gold ligaments and nanopore channels. (c) Histograms of scaled probability density of the diameters of gold ligaments and nanopore channels. Both distributions prove that gold ligaments and nanopore channels are topologically equivalent.

algorithm,[14] by which the volume of voxel data was digitally reduced from the surface, pixel by pixel, until skeletonized pixels remained at the center of nanopore channels or gold ligaments. For example, Fig. 3(a) shows the skeletonized gold ligaments. The various colors represent the deviation angles of the skeletonized ligaments from the z axis as indicated by the color bar from 0° (blue) to 90° (red). This skeletal network was used to measure each path length, i.e., gold ligament or nanopore channel length. The diameters of gold ligaments or nanopores were determined by counting removed pixels from the surface to the center of the ligaments on the skeletonal network. In this sample, the voxel dataset contains 2034 gold ligaments and 2480 nanopore channels. Figure 3(b) displays the distributions of path lengths for both gold ligaments and nanopore channels, which exhibit an asymmetric distribution with a broad maximum at ~15 nm and an average length of gold ligament and nanopore channel at 27 ± 12 and 26 ± 11 nm, respectively. Figure 3(c) illustrates the diameter distributions of gold ligaments and nanopore channels, which is found to follow a Gaussian dis-

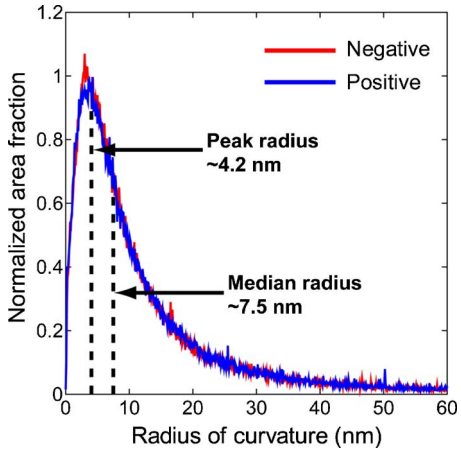

FIG. 4. (Color online) Normalized area fractions plotted against radius of curvature of gold ligaments. The red and blue lines represent negative and positive curvatures, respectively. The good agreement of the both lines indicates the net zero curvature of nanoporous gold by dealloying on average. The dash lines indicate the peak value at ~4.2 nm and the median curvature at ~7.5 nm.

tribution. The average diameters of the gold ligaments and nanopore channels were determined to be 11 ± 4.3 and 13 ± 6.6 nm, respectively. The aspect ratios of gold ligaments and nanopore channels are approximately between 2 and 3 and, thus, the structure of nanoporous gold can be rationally described as a quasiperiodic network comprised of randomly oriented gold nanowires and hollow nanochannels. Figures 3(b) and 3(c) suggest that the gold ligaments and nanopore channels are identical geometrically, which is different from the 3D morphology of the electrochemically dealloyed $Au_{20}Ag_{80}$.[6] In the case of $Au_{20}Ag_{80}$, the mean pore size is about twice as large as the ligament size, resulting in the volume fraction of gold ligaments is about 0.24. This dramatic divergence suggests that the morphology and topology of nanoporous gold strongly depend on the composition of precursor alloys and, probably, the dealloying conditions, which is consistent with the conventional SEM and TEM observations.[15,16]

One more quantitative analysis we have performed is the measurements of the principal curvature distribution of gold ligaments using local software. Such measurements are important because all surface mass transport in nanoporous gold is driven by the Gibbs–Thompson effect, i.e., the local chemical potential is proportional to the local radius of curvature.[17] In this study, the local curvatures were calculated by first translating the voxel data into isosurface data with triangular mesh by defining the distinct nanopore regions to the zero level, and then smoothening the surface data using a standard volume-conserving method.[18] The tensor of curvature at each node of the triangular mesh was calculated using a polyhedral approximation,[19] and the two principal radii of curvature at each node were found as the eigenvalues of the curvature tensor. The area of each node on the surface was calculated using a Voronoi cell construction. This allowed us to plot a histogram of the area fraction (of surface with local principal radius of curvature r) versus r, as shown in Fig. 4. The morphology of each nanoporous gold ligament contains both convexities (positive r) and concavities (negative r). Interestingly, the relative area fractions of each are equivalent, suggesting that the morphology of the nanoporous gold is close to a net zero-curvature surface, which is one of the common features of the bicontinuous structure.[20] The curvature distributions also show a sharp peak centered at $|r| \sim 4.2$ nm. This value appears to disagree with the average ligament radius, ~7.5 nm, measured by Fourier transform [Fig. 2(c)]. However, the median surface curvature of the distributions is found to be ~7.5 nm, well consistent with the average value estimated by using chords. This agreement indicates that the algorithm used for determining local curvatures is reliable. The discrepancy between the median and peak curvature values in Fig. 4 suggests that much of the surface dynamics (curvature-driven surface diffusion) is controlled by the features with higher curvatures than the apparent ligament diameter. It was reported that the 3D structure of the electrochemically dealloyed $Au_{20}Ag_{80}$ had convex surfaces.[6] However, the convex faces have not been seen in our samples prepared by dealloying $Au_{35}Ag_{65}$ alloy. Thus, further study may be required for fully understating the composition effect of precursor alloys on the 3D morphology of nanoporous gold. It is worth noting that the nanoporous gold is a highly active and biocompatible substrate for surface-enhanced Raman scattering (SERS) and the enhancement is linearly proportional to the curvatures of nanopores.[10] The curvature distributions with a sharp maximum shown in Fig. 4 therefore explain the stronger SERS enhancement of nanoporous gold with smaller nanopore sizes that leads to the dramatic reduction in the peak values.[10]

[1] J. Erlebacher, M. J. Aziz, A. Karma, N. Dimitrov, and K. Sieradzki, Nature (London) **410**, 450 (2001).
[2] A. J. Forty, Nature (London) **282**, 597 (1979).
[3] R. Li and K. Sieradzki, Phys. Rev. Lett. **68**, 1168 (1992).
[4] R. C. Newman, S. G. Corcoran, J. Erlebacher, M. J. Aziz, and K. Sieradzki, MRS Bull. **24**, 24 (1999).
[5] T. Fujita, L. H. Qian, K. Inoke, and M. W. Chen, Proceedings of the 16th International Microscopy Congress, Sapporo, Japan, 2006 (unpublished), p. 1864.
[6] H. Rösner, S. Parida, D. Kramer, C. A. Volkert, and J. Weissmüller, Adv. Eng. Mater. **9**, 535 (2007).
[7] Y. Ding, A. Mathur, M. W. Chen, and J. Erlebacher, Angew. Chem., Int. Ed. **44**, 4002 (2005).
[8] V. Zielasek, B. Jurgens, C. Schulz, J. Biener, M. M. Biener, A. V. Hamza, and M. Baumer, Angew. Chem., Int. Ed. **45**, 8241 (2006).
[9] L. H. Qian, Y. Ding, T. Fujita, and M. W. Chen, Langmuir **24**, 4426 (2008).
[10] L. H. Qian, X. Q. Yan, T. Fujita, and M. W. Chen, Appl. Phys. Lett. **90**, 153120 (2007).
[11] T. Fujita and M. W. Chen, Jpn. J. Appl. Phys. **47**, 1161 (2008).
[12] W. E. Lorensen and H. E. Cline, Comput. Graph. **21**, 163 (1987).
[13] We measured the active internal surface area of the nanoporous gold films by using electrochemical method. The result of ~9–11 m^2/g is well consistent with our TEM tomography results and also fairly agree with the date of nanoporous Au wires [C. X. Ji and P. C. Searson, J. Phys. Chem. B **107**, 4494 (2003)].
[14] C. M. Ma and M. Sonka, Comput. Vis. Image Underst. **64**, 420 (1996).
[15] X. Lu, E. Bischoff, R. Spolenak, and T. J. Balk, Scr. Mater. **56**, 557 (2007).
[16] X. Y. Lang, L. H. Qian, T. Fujita, and M. W. Chen (unpublished).
[17] C. T. Campbell, S. C. Parker, and D. E. Starr, Science **298**, 811 (2002).
[18] G. Taubin, Proceedings of the Fifth International Conference on Computer Vision, 1995 (unpublished), p. 852.
[19] G. Taubin, Proceedings of the Fifth International Conference on Computer Vision, 1995 (unpublished), p. 902.
[20] H. Jinnai, T. Koga, Y. Nishikawa, T. Hashimoto, and S. T. Hide, Phys. Rev. Lett. **78**, 2248 (1997).